

Demonstration of the Highest Deuterium–Tritium Areal Density Using Triple-Picket Cryogenic Designs on OMEGA

In inertial confinement fusion (ICF) implosions, a cryogenic shell of deuterium–tritium (DT) fuel is driven inward by means of direct or indirect laser illumination to achieve high compression and burn.¹ Fuel burn proceeds in two stages: First, a lower-density, higher-temperature (~ 10 -keV) hot spot is formed by PdV work of converging higher-density, lower-temperature shells. Calculations show that to initiate burn, the shell kinetic energy must exceed the threshold value,² which depends on the shell implosion velocity V_{imp} (peak mass-averaged shell velocity), the in-flight shell adiabat α_{if} (ratio of shell pressure to the Fermi-degenerate pressure at the position in peak shell density), and the drive pressure p_{d} . Second, as burn propagates through the fuel, shell inertia provides sufficient confinement time to burn a significant fraction of the assembled fuel. This requires fuel areal densities (ρR) at peak compression in excess of ~ 0.9 g/cm² (Ref. 1). The peak areal density in a direct-drive implosion depends mainly on α_{if} and laser energy E_{L} (Ref. 3):

$$\max(\rho R)_{\text{g/cm}^2} = \frac{2.6 E_{\text{L,MJ}}^{1/3}}{\alpha_{\text{if}}^{0.54}}. \quad (1)$$

Therefore, to burn a sufficient fraction of the fuel, the shell adiabat must be $\alpha_{\text{if}} \leq 7 E_{\text{L,MJ}}^{0.6}$. While hot-spot formation and burn-initiation physics require laser energy in excess of ~ 300 kJ, which will be available on the National Ignition Facility (NIF),⁴ implosions on the OMEGA laser⁵ validate the ability of ignition designs to assemble cryogenic fuel with ignition-relevant implosion velocities ($V_{\text{imp}} > 3 \times 10^7$ cm/s), maintaining the required fuel adiabat. A deviation of the adiabat from the designed value in an implosion can be inferred by comparing the measured and predicted values of ρR . The areal density is determined by measuring spectral shapes of reaction products as they interact with the fuel.^{6,7} This gives a value $\langle \rho R \rangle_{\text{n}}$ averaged over reaction time history. The theoretical value of $\langle \rho R \rangle_{\text{n}}$ has a similar dependence on α_{if} and E_{L} as in Eq. (1) with a numerical factor of 1.7 instead of 2.6 (Ref. 3). Using this scaling, an OMEGA cryogenic-DT design, hydrodynamically equivalent to an $\alpha_{\text{if}} = 2$ ignition design on the NIF, is predicted to achieve $\langle \rho R \rangle_{\text{n}} \sim 300$ mg/cm² at a laser

energy ~ 25 to 30 kJ and a laser absorption fraction of 60% to 70%, typical for OMEGA-scale targets. Reaching these areal densities on OMEGA, therefore, is a crucial step in validating predictive capabilities of hydrodynamic codes used to design ignition targets on the NIF.

The shell adiabat is determined by heating sources, including shock waves, radiation, and suprathermal electrons. Because of inaccuracies in the models used to design targets, experimental tuning is required to ensure that preheat is at an acceptable level. This article describes direct-drive target designs optimized for experimental shock timing to prevent adiabat degradation caused by excessive shock heating. This is accomplished by combining three intensity pickets with the main drive pulse [triple-picket (TP) design]. The main pulse in this case requires minimal shaping (an intensity step is introduced to control the strength of the main shock). Areal densities up to 300 mg/cm² are observed in cryogenic-DT implosions on OMEGA using the TP designs driven at peak intensities $\sim 8 \times 10^{14}$ W/cm².

One of the main challenges in designing hot-spot ignition implosions is to control the generation of strong shocks while accelerating the fuel shell to high implosion velocities. To avoid excessive shock heating, only few-Mbar shocks can be launched into cryogenic fuel at the beginning of an implosion. On the other hand, reaching $V_{\text{imp}} > 3 \times 10^7$ cm/s without the Rayleigh–Taylor instability⁸ disrupting the shell requires drive pressures p_{d} in excess of 100 Mbar since the shell’s in-flight aspect ratio A_{in} (ratio of shell radius R to shell thickness) is proportional to $p_{\text{d}}^{-2/5}$ (Ref. 3) and shells with higher A_{in} are more susceptible to perturbation growth during the acceleration phase. Such a pressure increase from a few Mbar to 100 Mbar can be achieved either adiabatically [continuous-pulse (CP) design]^{9,10} or by launching a sequence of shocks of increasing strength [multiple-shock (MS) designs].^{1,11}

Early cryogenic spherical implosions on OMEGA used the CP designs.^{12–15} Both 5- and 10- μm -thick CD shells with cryogenic 95- μm -thick D₂ and 80- μm -thick DT layers were

used in these experiments. Areal densities close to the predicted values ($\langle \rho R \rangle_n \sim 100$ to 120 mg/cm²) were achieved in implosions with 5- μ m shells driven at peak intensities below $I_{\text{limit}} = 3 \times 10^{14}$ W/cm² ($p_d \sim 50$ Mbar) and a laser pulse contrast ratio (CR) of less than 3.5. When 10- μ m shells were used, $\langle \rho R \rangle_n$ values up to 200 mg/cm² (80% to 90% of the predicted areal densities) were measured for designs with $I_{\text{limit}} = 5 \times 10^{14}$ W/cm² ($p_d \sim 75$ Mbar) and a CR < 30 (Ref. 15). The implosion velocity was $V_{\text{imp}} \simeq 2.2 \times 10^7$ cm/s. Increasing drive intensities above I_{limit} resulted in significant deviations of measured and predicted $\langle \rho R \rangle_n$ (Ref. 14). Shock velocity measured in the CP designs using a velocity interferometry system for any reflector (VISAR)¹⁶ revealed difficulty in reproducing an adiabatic compression wave predicted in simulations.^{14,17} Since the effect of steepening a compression wave into a shock, not predicted in simulations, is exacerbated by increasing either peak drive intensity or laser pulse CR, it is impractical to experimentally tune the adiabat in the CP designs to ignition-relevant values.

Initial fuel compression prior to reaching peak drive intensity can be accurately controlled in the MS designs by launching a sequence of shocks using intensity pickets. Here we describe the main features of such designs. First, we assume that N shocks are launched by narrow pickets (picket duration is much shorter than shock transit time across the shell), and the main shock is launched and supported by the main pulse. Since pressure of an unsupported shock decays in time, the fuel adiabat decreases from the front to the back of the shell. Equation (1) needs to be modified in this case to reflect spatial variation in α_{if} . The following supports using only the adiabat at the inner shell surface (“inner adiabat” α_{inn}) to determine areal density.³ The maximum shell convergence during an implosion is limited by a rarefaction wave, created at the main shock-breakout time, with a tail propagating from the inner part of the shell toward the target center. Since material in a rarefaction moves at the local sound speed with respect to position of the peak shell density, the low-density tail is larger if the inner adiabat is higher. Later, as the main shock reflects from the center and begins interacting with the rarefaction, pressure at the target center starts to build up, initiating shell deceleration. Therefore, the larger the inner adiabat, the larger the rarefaction region, causing the main shell to decelerate farther from the center, thereby reducing the final shell convergence and areal density.

Since the adiabat is proportional to pressure over density to the 5/3rd power, shocks launched by the pickets must raise the inner shell density to a value sufficient to keep the main

shock with $p_d \sim 100$ Mbar from increasing the inner adiabat above the required value. To maximize this compression, all shocks must coalesce nearly simultaneously in the vapor region, soon after they break out of the shell. This relates the picket amplitudes and timing. Using the adiabat relation with pressure and density ρ in DT fuel, $\alpha \simeq p(\text{Mbar})/2.16 \rho^{5/3}$, the required inner shell compression after the main shock can be written as $\rho_{\text{main}}/\rho_0 \simeq 40[(p_d/100 \text{ Mbar})/\alpha_{\text{inn}}]^{3/5}$, where $\rho_0 = 0.25$ g/cm³ is the initial shell density. The density at the first shock front is compressed by a factor of ~ 4 if shock pressure p_1 stays above ~ 1 Mbar. Maximizing the density compression by the remaining N shocks ($N-1$ shocks from pickets and the main shock) leads, with the help of Hugoniot relations,¹⁸ to a condition on shock-pressure ratio as the shocks reach the inner surface, $p_{i+1} = p_i(p_d/p_1)^{1/N}$, where $i = 1, \dots, N$. The inner adiabat in this case is

$$\alpha_{\text{inn}} = 46.3 \left(\frac{p_d}{100 \text{ Mbar}} \right) \left[\frac{(p_d/p_1)^{1/N} + 4}{4(p_d/p_1)^{1/N} + 1} \right]^{5N/3}. \quad (2)$$

Because of radiation preheat and additional heating caused by a secondary compression wave formed at the beginning of shell acceleration, the in-flight adiabat used in Eq. (1) is higher than α_{inn} predicted by Eq. (1). In general, for an optimized multiple-picket design, an effective α_{inn} is larger by a factor of 2 to 2.5. Therefore, a high-yield, direct-drive NIF design requires that the number N of pickets be determined by setting $\alpha_{\text{inn}} \simeq 1$ (which is equivalent to an $\alpha \simeq 2.5$ CP design) in Eq. (2). This gives a relation between N and p_d , which can be approximated by $p_d(\text{Mbar}) \simeq 6.5 N e^{0.78 N}$. For $p_d \sim 100$ Mbar, this gives $N = 3$, and pressures of the first three shocks as they break out of the shell are 1, 4.6, and 21 Mbar, respectively.

Next, a simple model is used to gain insight into the shock evolution in a multiple-picket design. A shock wave traveling along the x axis with a velocity U_{sh} is assumed to be strong enough that the flow velocity ahead of the shock can be neglected with respect to post-shock velocity in the laboratory frame of reference. Using the ideal-gas equation-of-state model, the mass density in this case increases by a factor of 4 across the shock front. Gradients in the flow created by unsupported shocks lead to PdV work on a fluid element, $d_t p \equiv \partial_t p + v \partial_x p = -(5/3)p \partial_x v$. The spatial gradient in velocity can be expressed in terms of pressure gradient and acceleration in the shock-front frame using Bernoulli’s relation $v \partial_x v + \partial_x p/\rho = -d_t U_{\text{sh}} - \partial_t v$. In the strong-shock limit, $v = -U_{\text{sh}}/4$ and $U_{\text{sh}} = \sqrt{(4/3)p_{\text{sh}}/\rho_0}$, leading to $d_t(p_{\text{sh}} U_{\text{sh}}^5) = -U_{\text{sh}}^6 (\partial_x p)_{\text{sh}}$, where p_{sh} is shock pressure and ρ_0 is density ahead of the shock. This equation can

be simplified by introducing a mass coordinate, $dm = \rho dx$, and replacing time with the mass m_{sh} overtaken by the shock, $dm_{\text{sh}} = \rho U_{\text{sh}} dt$. At the shock front, this gives

$$\frac{d \ln(p_{\text{sh}} U_{\text{sh}}^5)}{dm_{\text{sh}}} = -4 \left(\frac{\partial \ln p}{\partial m} \right)_{\text{sh}}. \quad (3)$$

According to a self-similar solution¹⁹ and simulation results, the pressure behind the unsupported shock changes nearly linearly with mass, $p \sim m$. In this case, Eq. (3) gives $p_{\text{sh}} \sim m_{\text{sh}}^{-1.14} \rho_0^{0.71}$. The first shock travels through uniform density; therefore, the shock pressure decays as $p_1 \sim m_{\text{sh}}^{-1.14}$ and the post-shock adiabat varies as $\alpha_1 \sim m^{-1.14}$. Compared to the results of a self-similar solution,¹⁹ the error in the power index predicted by this model is within 10%. The density after the shock evolves as $\rho \sim (p/\alpha_1)^{3/5}$. Therefore, as the second shock is launched, the density ahead of its front grows as $\rho_0 \sim m_{\text{sh}}^{1.29}$ and shock pressure decays as $p_2 \sim m_{\text{sh}}^{-0.22}$. To generalize, if an $i + 1$ shock with $p_{i+1} \sim m_{\text{sh}}^{\delta_{i+1}}$ travels through the flow with an adiabat profile $\alpha_i \sim m^{-\omega_i}$, the model gives $\delta_{i+1} = 0.57 \delta_i + 0.43$ and $\omega_{i+1} = 0.57 \omega_i + 1.71$ with $\delta_1 = -\omega_1 = -1.14$. Therefore, starting with the third shock, the pressure at the unsupported shock front increases as the shock travels through the shell. For the main shock launched after N decaying shocks and supported by pressure p_d , Eq. (3) gives (assuming that pressure changes linearly with the mass coordinate)

$$p_{\text{main}} = p_d \left[3(\omega_N + 1) \left(m_{\text{sh}} / m^* \right)^{\delta_{N+1}} - 8 \right] / (3\omega_N - 5),$$

where m^* is a normalization constant that depends on picket duration.

The model shows that the main shock pressure increases as the shock propagates through the shell, significantly exceeding the ablation pressure. To avoid an increase in the inner adiabat caused by this pressure amplification, it is necessary to either increase the number of pickets to 4 or reduce the strength of the main shock by introducing an intensity step at the beginning of the main drive. Since incorporating the fourth picket in the design is very challenging because of the short time separation between the last picket and the main drive, a combination of three pickets and a step pulse is chosen as a baseline for the multiple-picket, low-adiabat designs.

As mentioned earlier, all shocks launched by the pickets and the main drive must coalesce nearly simultaneously in the vapor region of the target, in close proximity to the inner shell surface.

A VISAR measurement in an optimized design should produce, therefore, a decaying velocity of the first shock, followed by a rapid velocity increase, at the coalescence time, up to a value above $\sim 120 \mu\text{m/ns}$ (see the dotted line in Fig. 121.1). Because of the radiative precursor, the VISAR signal is absorbed in a region ahead of the shock front if $V_{\text{sh}} > 75 \mu\text{m/ns}$ (Ref. 20). As a result, only the first shock velocity and time of shock coalescence can be measured by the VISAR. Deviations from the predicted strength of any shock can be inferred by observing multiple jumps in the velocity of the leading shock wave. For example, if the third picket is too high, the third shock will prematurely overtake the second and first shocks, resulting in an early velocity jump, as shown in Fig. 121.1. The measurement presented in Fig. 121.1 was performed on OMEGA with a $900\text{-}\mu\text{m}$ -diam, $10\text{-}\mu\text{m}$ -thick CD shell filled with liquid D_2 and fitted with a VISAR cone.¹⁷ As seen in Fig. 121.1, the two coalescence events, separated by ~ 300 ps, are a signature of mistimed shocks that can be corrected by reducing the intensity of the third picket.

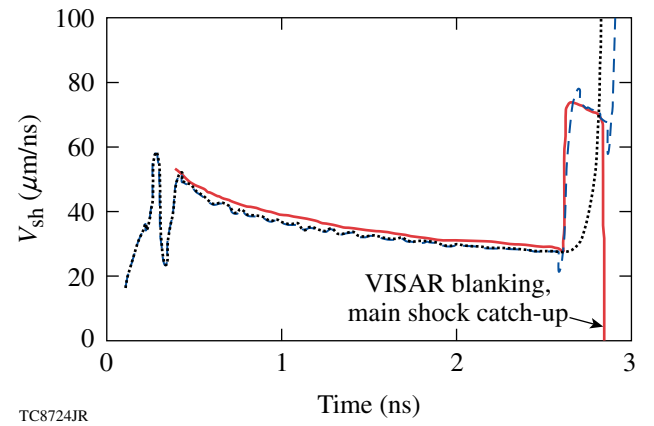


Figure 121.1

Example of leading shock-velocity history measured (red line) and predicted (dashed line) in the TP design with a mistimed third shock. The calculated velocity history for an optimized design is shown by the dotted line.

To verify the shock optimization procedure and validate control of the main shock strength with an intensity step, the TP designs with both square and step main pulses were used on OMEGA to drive targets with a $65\text{-}\mu\text{m}$ -thick cryogenic-DT layer overcoated with a $10\text{-}\mu\text{m}$ CD shell. The pulse shapes shown in Fig. 121.2 had a peak intensity of $\sim 8 \times 10^{14} \text{ W/cm}^2$. The laser energy varied from 23 kJ for the square main pulse to 25 kJ for the step main pulse, respectively. The predicted implosion velocity in these designs reached $V_{\text{imp}} = 3 \times 10^7 \text{ cm/s}$. A magnetic recoil spectrometer (MRS)⁶ was used to infer $\langle \rho R \rangle_n$. Two charged-particle spectrometers (CPS's) were also used to

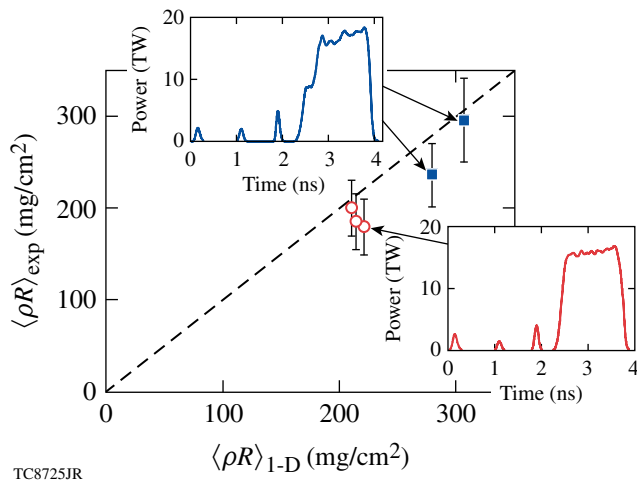


Figure 121.2

Predicted and measured areal densities for triple-picket square (circles) and step (squares) OMEGA designs. The inserts show the pulse shapes used to drive the implosions.

measure the spectral shape of the knock-on deuterons (KOD's), elastically scattered by primary DT neutrons. The shape in the KOD spectrum is insensitive, however, to areal densities above $\langle \rho R \rangle_n > 180 \text{ mg/cm}^2$ (Ref. 6). These measurements were used to infer the lower limit on $\langle \rho R \rangle_n$ as well as assess asymmetries developed at different views of an implosion. In Fig. 121.2 the measured areal densities are compared to those calculated using the one-dimensional hydrocode *LILAC*.²¹ Good agreement between measurements and calculations validates the accuracy of shock tuning in the TP designs. Also, the observed increase in $\langle \rho R \rangle_n$ in the step design confirms that the inner adiabat can be accurately controlled by changing step amplitude in the main drive.

Based on the good performance of the TP designs on OMEGA, a new triple-picket, direct-drive-ignition design is proposed for the NIF (Fig. 121.3). Driven at a peak intensity of $8 \times 10^{14} \text{ W/cm}^2$, the shell reaches $V_{\text{imp}} = 3.5$ to $4 \times 10^7 \text{ cm/s}$, depending on the thickness of the fuel layer. At a laser energy of 1.5 MJ, this design is predicted to ignite with a gain $G = 48$. A stability assessment of the NIF TP design is currently in progress.

In summary, triple-picket designs were used in cryogenic-DT implosions on OMEGA. The highest areal densities ever measured in cryogenic-DT implosions (up to 300 mg/cm^2) were inferred with $V_{\text{imp}} \sim 3 \times 10^7 \text{ cm/s}$ driven at a peak laser intensity of $8 \times 10^{14} \text{ W/cm}^2$. Scaled to the NIF, the TP design is predicted to ignite with a gain $G = 48$.

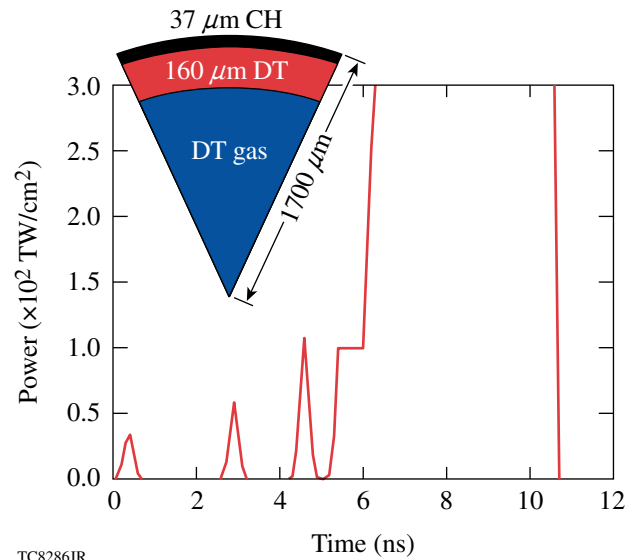


Figure 121.3

Triple-picket, direct-drive design for the NIF.

ACKNOWLEDGMENT

This work was supported by the U.S. Department of Energy Office (DOE) of Inertial Confinement Fusion under Cooperative Agreement No. DE-FC52-08NA28302, the University of Rochester, and the New York State Energy Research and Development Authority. The support of DOE does not constitute an endorsement by DOE of the views expressed in this article.

REFERENCES

1. J. D. Lindl, *Inertial Confinement Fusion: The Quest for Ignition and Energy Gain Using Indirect Drive* (Springer-Verlag, New York, 1998).
2. M. C. Herrmann, M. Tabak, and J. D. Lindl, *Phys. Plasmas* **8**, 2296 (2001).
3. C. D. Zhou and R. Betti, *Phys. Plasmas* **14**, 072703 (2007).
4. J. Paisner *et al.*, *Laser Focus World* **30**, 75 (1994).
5. T. R. Boehly, D. L. Brown, R. S. Craxton, R. L. Keck, J. P. Knauer, J. H. Kelly, T. J. Kessler, S. A. Kumpan, S. J. Loucks, S. A. Letzring, F. J. Marshall, R. L. McCrory, S. F. B. Morse, W. Seka, J. M. Soures, and C. P. Verdon, *Opt. Commun.* **133**, 495 (1997).
6. J. A. Frenje, C. K. Li, F. H. Séguin, D. T. Casey, R. D. Petrasso, T. C. Sangster, R. Betti, V. Yu. Glebov, and D. D. Meyerhofer, *Phys. Plasmas* **16**, 042704 (2009).
7. F. H. Séguin, C. K. Li, J. A. Frenje, D. G. Hicks, K. M. Green, S. Kurebayashi, R. D. Petrasso, J. M. Soures, D. D. Meyerhofer, V. Yu. Glebov, P. B. Radha, C. Stoeckl, S. Roberts, C. Sorce, T. C. Sangster, M. D. Cable, K. Fletcher, and S. Padalino, *Phys. Plasmas* **9**, 2725 (2002).
8. S. Chandrasekhar, in *Hydrodynamic and Hydromagnetic Stability*, International Series of Monographs on Physics (Clarendon Press, Oxford, 1961), p. 428.

9. P. W. McKenty, V. N. Goncharov, R. P. J. Town, S. Skupsky, R. Betti, and R. L. McCrory, *Phys. Plasmas* **8**, 2315 (2001).
10. V. N. Goncharov, J. P. Knauer, P. W. McKenty, P. B. Radha, T. C. Sangster, S. Skupsky, R. Betti, R. L. McCrory, and D. D. Meyerhofer, *Phys. Plasmas* **10**, 1906 (2003).
11. J. D. Lindl and W. C. Mead, *Phys. Rev. Lett.* **34**, 1273 (1975).
12. F. J. Marshall, R. S. Craxton, J. A. Delettrez, D. H. Edgell, L. M. Elasky, R. Epstein, V. Yu. Glebov, V. N. Goncharov, D. R. Harding, R. Janezic, R. L. Keck, J. D. Kilkenny, J. P. Knauer, S. J. Loucks, L. D. Lund, R. L. McCrory, P. W. McKenty, D. D. Meyerhofer, P. B. Radha, S. P. Regan, T. C. Sangster, W. Seka, V. A. Smalyuk, J. M. Soures, C. Stoeckl, S. Skupsky, J. A. Frenje, C. K. Li, R. D. Petrasso, and F. H. Séguin, *Phys. Plasmas* **12**, 056302 (2005).
13. T. C. Sangster, R. Betti, R. S. Craxton, J. A. Delettrez, D. H. Edgell, L. M. Elasky, V. Yu. Glebov, V. N. Goncharov, D. R. Harding, D. Jacobs-Perkins, R. Janezic, R. L. Keck, J. P. Knauer, S. J. Loucks, L. D. Lund, F. J. Marshall, R. L. McCrory, P. W. McKenty, D. D. Meyerhofer, P. B. Radha, S. P. Regan, W. Seka, W. T. Shmayda, S. Skupsky, V. A. Smalyuk, J. M. Soures, C. Stoeckl, B. Yaakobi, J. A. Frenje, C. K. Li, R. D. Petrasso, F. H. Séguin, J. D. Moody, J. A. Atherton, B. D. MacGowan, J. D. Kilkenny, T. P. Bernat, and D. S. Montgomery, *Phys. Plasmas* **14**, 058101 (2007).
14. V. A. Smalyuk, R. Betti, T. R. Boehly, R. S. Craxton, J. A. Delettrez, D. H. Edgell, V. Yu. Glebov, V. N. Goncharov, D. R. Harding, S. X. Hu, J. P. Knauer, F. J. Marshall, R. L. McCrory, P. W. McKenty, D. D. Meyerhofer, P. B. Radha, S. P. Regan, T. C. Sangster, W. Seka, R. W. Short, D. Shvarts, S. Skupsky, J. M. Soures, C. Stoeckl, B. Yaakobi, J. A. Frenje, C. K. Li, R. D. Petrasso, and F. H. Séguin, *Phys. Plasmas* **16**, 056301 (2009).
15. T. C. Sangster, V. N. Goncharov, P. B. Radha, V. A. Smalyuk, R. Betti, R. S. Craxton, J. A. Delettrez, D. H. Edgell, V. Yu. Glebov, D. R. Harding, D. Jacobs-Perkins, J. P. Knauer, F. J. Marshall, R. L. McCrory, P. W. McKenty, D. D. Meyerhofer, S. P. Regan, W. Seka, R. W. Short, S. Skupsky, J. M. Soures, C. Stoeckl, B. Yaakobi, D. Shvarts, J. A. Frenje, C. K. Li, R. D. Petrasso, and F. H. Séguin, *Phys. Rev. Lett.* **100**, 185006 (2008).
16. L. M. Barker and R. E. Hollenbach, *J. Appl. Phys.* **43**, 4669 (1972).
17. T. R. Boehly, D. H. Munro, P. M. Celliers, R. E. Olson, D. G. Hicks, V. N. Goncharov, G. W. Collins, H. F. Robey, S. X. Hu, J. A. Marozas, T. C. Sangster, O. L. Landen, and D. D. Meyerhofer, *Phys. Plasmas* **16**, 056302 (2009).
18. L. D. Landau and E. M. Lifshitz, *Fluid Mechanics*, 2nd ed., Course of Theoretical Physics, Vol. 6 (Butterworth-Heinemann, Newton, MA, 1987).
19. Ya. B. Zel'dovich and Yu. P. Raizer, in *Physics of Shock Waves and High-Temperature Hydrodynamic Phenomena*, edited by W. D. Hayes and R. F. Probstein (Dover Publications, Mineola, NY, 2002), Vol. II, Chap. XII, pp. 820–848.
20. D. H. Munro *et al.*, *Phys. Plasmas* **8**, 2245 (2001).
21. J. Delettrez, R. Epstein, M. C. Richardson, P. A. Jaanimagi, and B. L. Henke, *Phys. Rev. A* **36**, 3926 (1987).